Electronic Supplementary Material (ESI) for Journal of Materials Chemistry A.

Tailoring the Hetero-Structure of Iron Oxides in the Framework of Nitrogen Doped Carbon for Oxygen Reduction Reaction and Zinc-Air Battery

Zhourong Xiao[a], Chan Wu[a], Wei Wang[a], Lun Pan[a,b], Jijun Zou[a,b], Li Wang[a,b], Xiangwen Zhang[a,b], Guozhu Li[a,b]*

[a] Key Laboratory for Green Chemical Technology of Ministry of Education, School of Chemical Engineering and Technology, Tianjin University, Tianjin 300072, China

[b] Collaborative Innovation Center of Chemical Science and Engineering (Tianjin), Tianjin 300072, China

*Corresponding author. Tel. /fax: +86 22 27892340.

E-mail address: gzli@tju.edu.cn

Electrochemical measurement

CompactStat.h10800 potentiostat/galvanostat/electrochemical analyser (Ivium Technologies Co., Netherland), combining with a rotation speed controller (Pine Instrument Co., USA), was employed to perform the electrochemical measurement. A three-electrode system was set up and used for electrochemical data collection. RHE was used as the reference electrode, a graphite rod was selected as the counter electrode, and the catalyst-coated GCE was served as the working electrode, respectively.

Cyclic voltammetry (CV) curves were collected in O_2-saturated or Ar-saturated KOH solution (0.1 M) at a scan rate of 50 mV s^{-1} from 0.164 V to 1.164 V (vs RHE, the potential is relative to RHE unless specifically illustrated hereinafter). The polarization plots for ORR (linear sweep voltammetry, LSV) were obtained using the rotating disk electrode (RDE) technique in O_2-saturated KOH solution (0.1 M). Commercial Pt/C (20 wt%) was obtained from HeSen Electric Co., and used as the benchmark.

The number of electrons transferred per O_2 molecule (n) in ORR was calculated using Koutecky-Levich (K-L) equation listed below.

$$\frac{1}{J} = \frac{1}{J_L} + \frac{1}{J_K} = \frac{1}{B\omega^{1/2}} + \frac{1}{nFkC_0}$$

$$B = 0.2nFC_0D_0^{2/3}\nu^{-1/6}$$

Where J_L is the limiting diffusion current density (mA cm^{-2}), J is the measured current density (mA cm^{-2}), F is the Faraday constant (96485 C mol^{-1}), ω is the rotating speed (rpm), C_0 is the bulk concentration of O_2 (1.2×10^{-6} mol cm^{-3}), ν is the kinetic viscosity of the electrolyte (0.01 cm^2 s^{-1}), k is the electron-transfer rate constant, and D_0 is the O_2 diffusion coefficient (1.9×10^{-5} cm^2 s^{-1}).

The electron transfer number (n) and hydrogen peroxide yield (H_2O_2 %) were verified based on ring current (I_{ring}) and disk current (I_{disk}) by RRDE measurement at 1600 rpm.

Where N, representing the collection efficiency of Pt ring, equals to 0.37.

$$n = 4 \times \frac{I_{disk}}{(I_{disk} + I_{ring}/N)}$$

$$H_2O_2\,\% = 200 \times \frac{I_{ring}/N}{(I_{disk} + I_{ring}/N)}$$

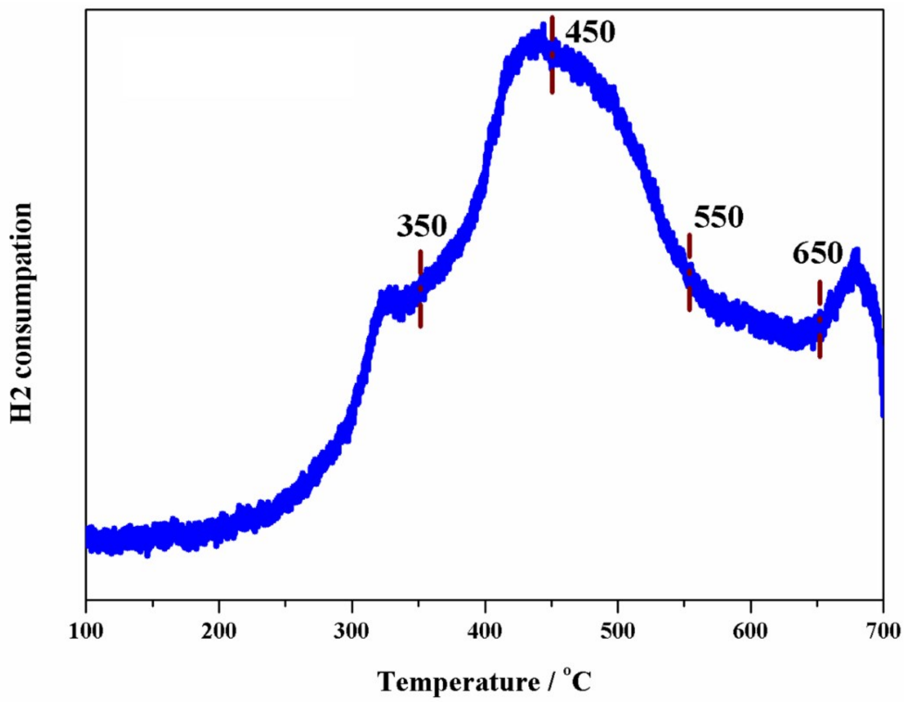

Figure. S1 TPR profile of Fe_2O_3@NC-0.

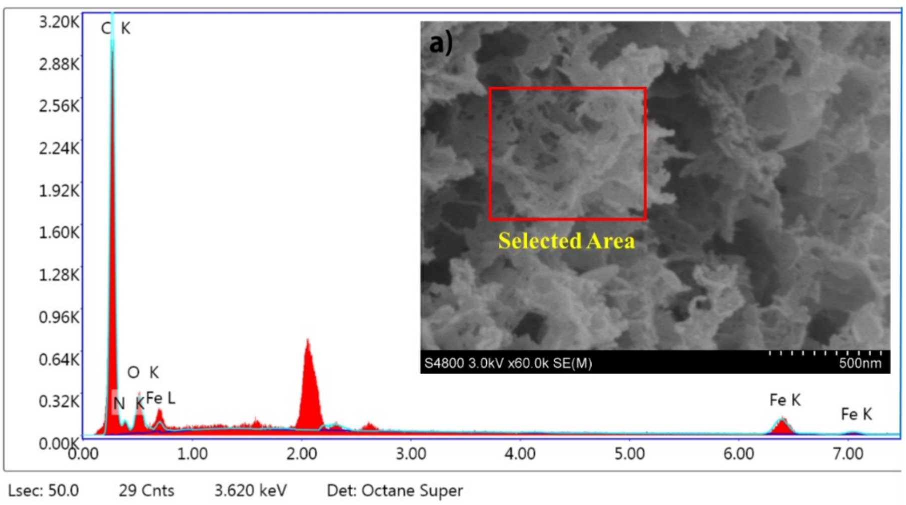

Figure. S2 SEM image of the as-prepared Fe_2O_3@NC-450 and corresponding EDX spectrum.

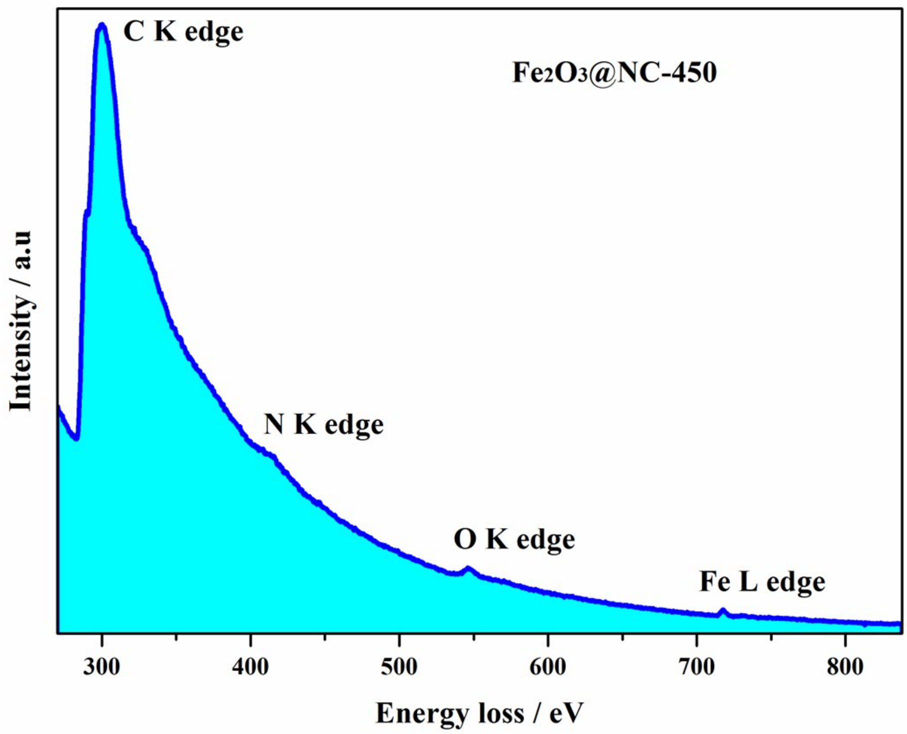

Figure. S3 EELS spectrum of the as-prepared Fe_2O_3@NC-450.

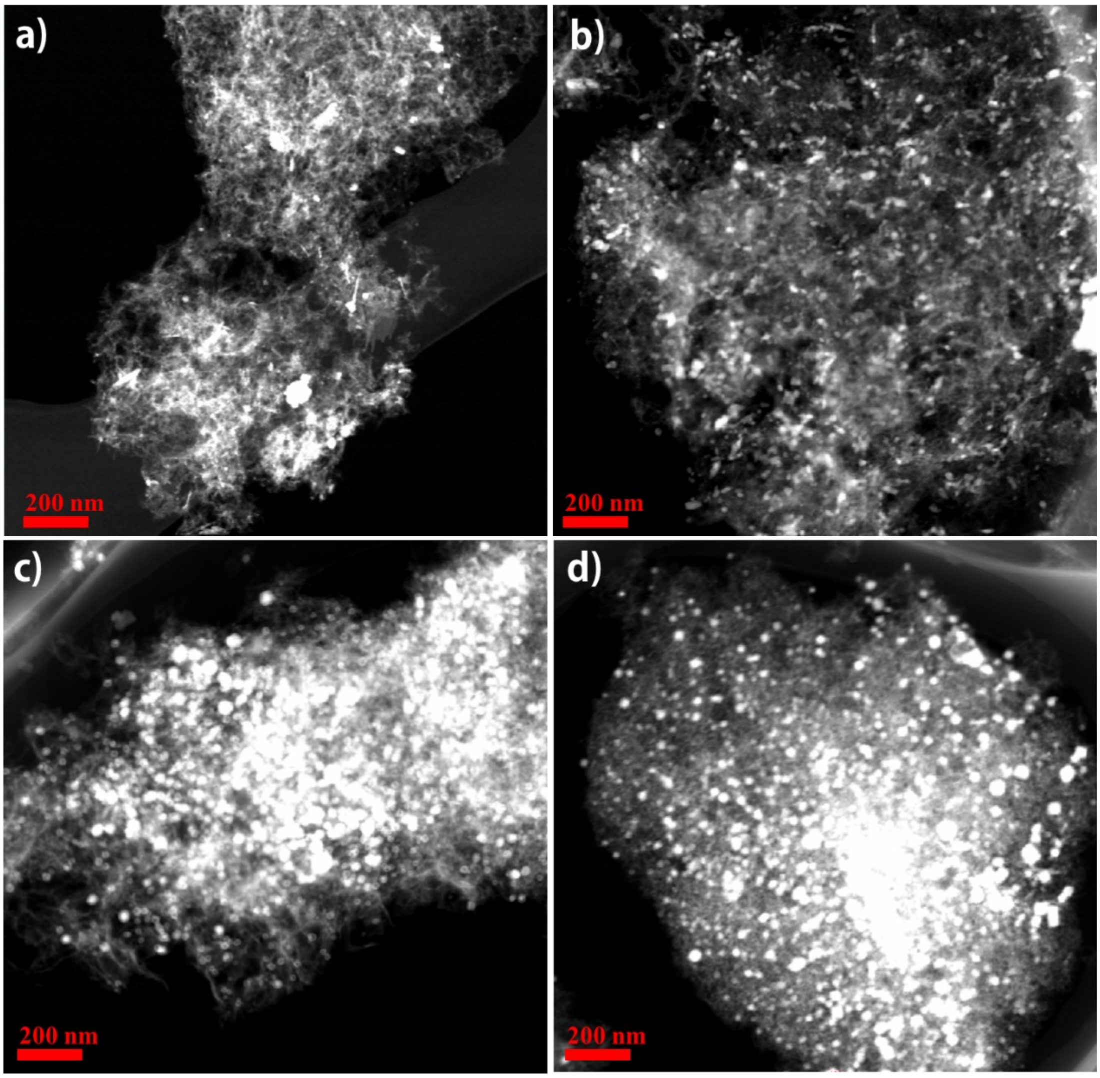

Figure. S4 HAADF-STEM images of the as-prepared samples. (a) Fe_2O_3@NC-0, (b) Fe_2O_3@NC-350, (c) Fe_2O_3@NC-550 and (d) Fe_2O_3@NC-650.

.

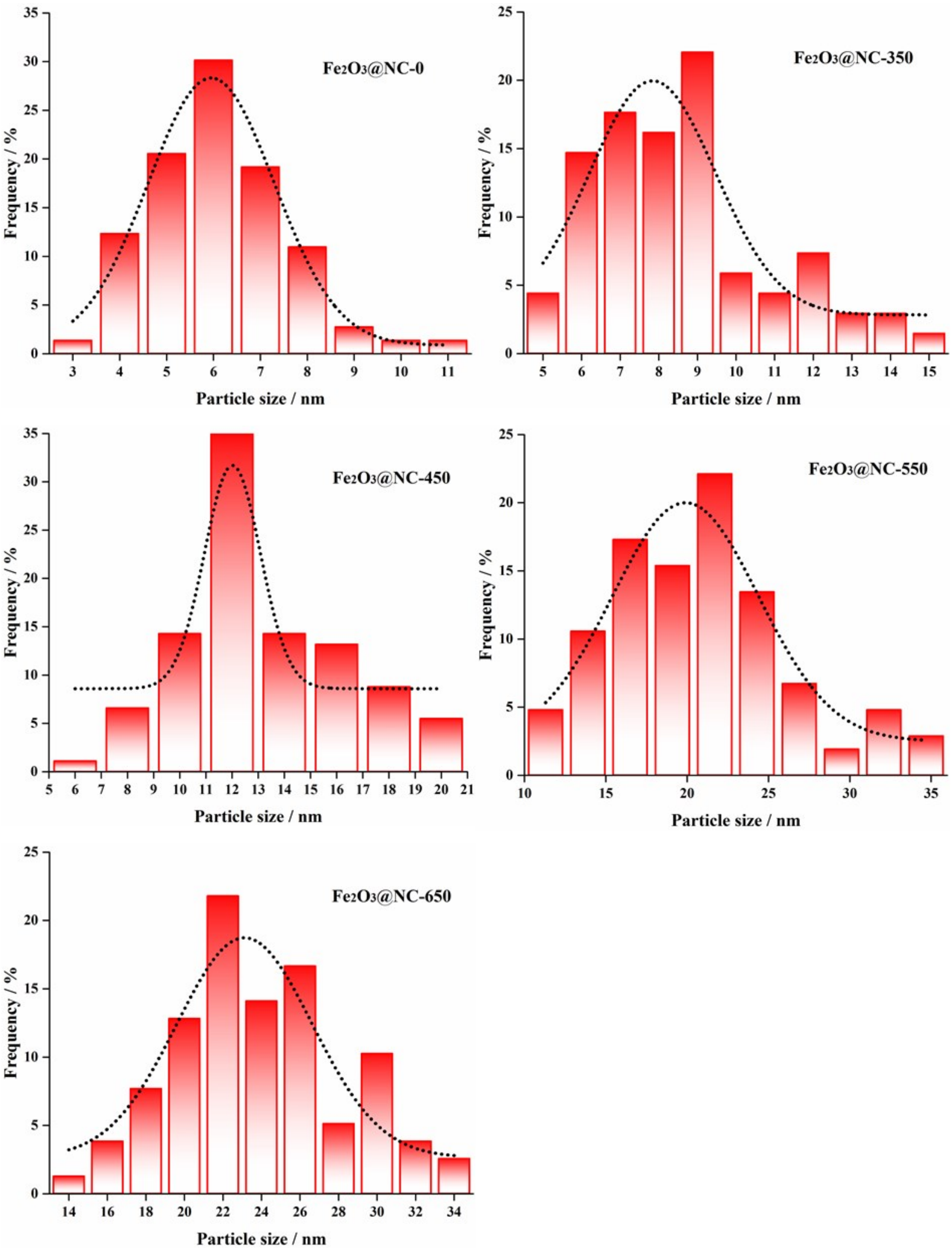

Figure. S5 Particle size distribution of iron species in the as-prepared catalysts.

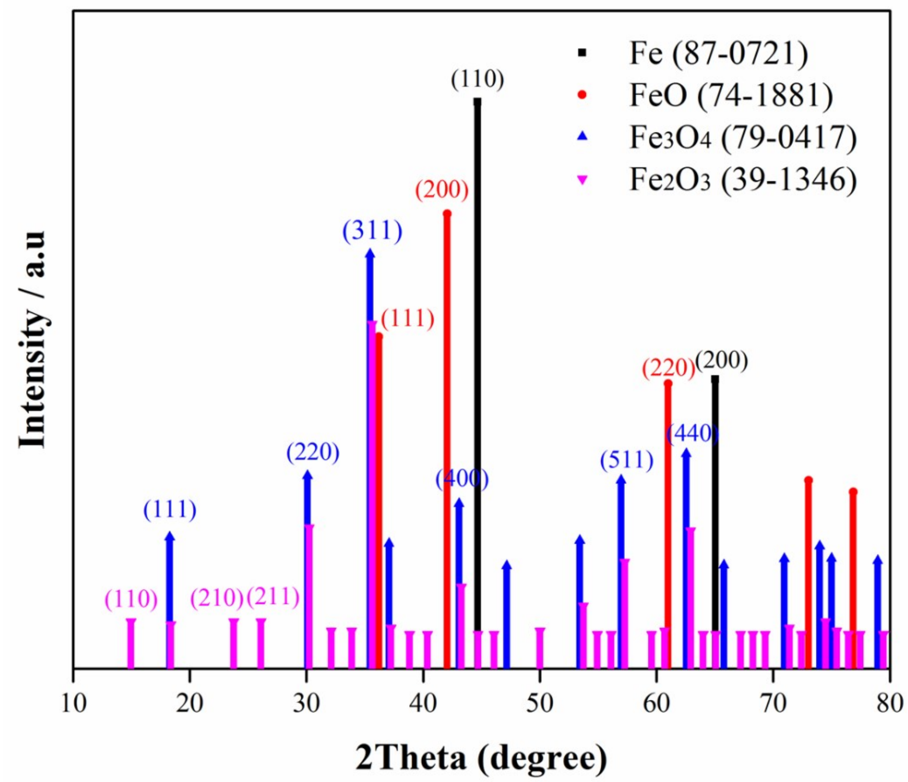

Figure. S6 Standard XRD patterns of different iron species (FeO_x).

Table S1 - Textural properties of the as-prepared catalysts.

Catalysts	BET Surface Area (m^2/g)	Pore Volume (cm^3/g)	Average Pore Size (nm)	Iron oxides particle size (nm)[a]	I_D/I_G[b]
Fe_2O_3@NC-0	1366.3	1.81	9.76	6	1.02
Fe_2O_3@NC-350	1399.3	1.71	7.68	9	1.00
Fe_2O_3@NC-450	1432.3	1.61	7.59	12	1.01
Fe_2O_3@NC-550	1336.8	1.65	7.54	20	1.02
Fe_2O_3@NC-650	1289.9	1.60	7.56	23	1.01

[a] Average particle size of iron species was measured from TEM images.

[b] According to Raman results and using the peak intensity ratio.

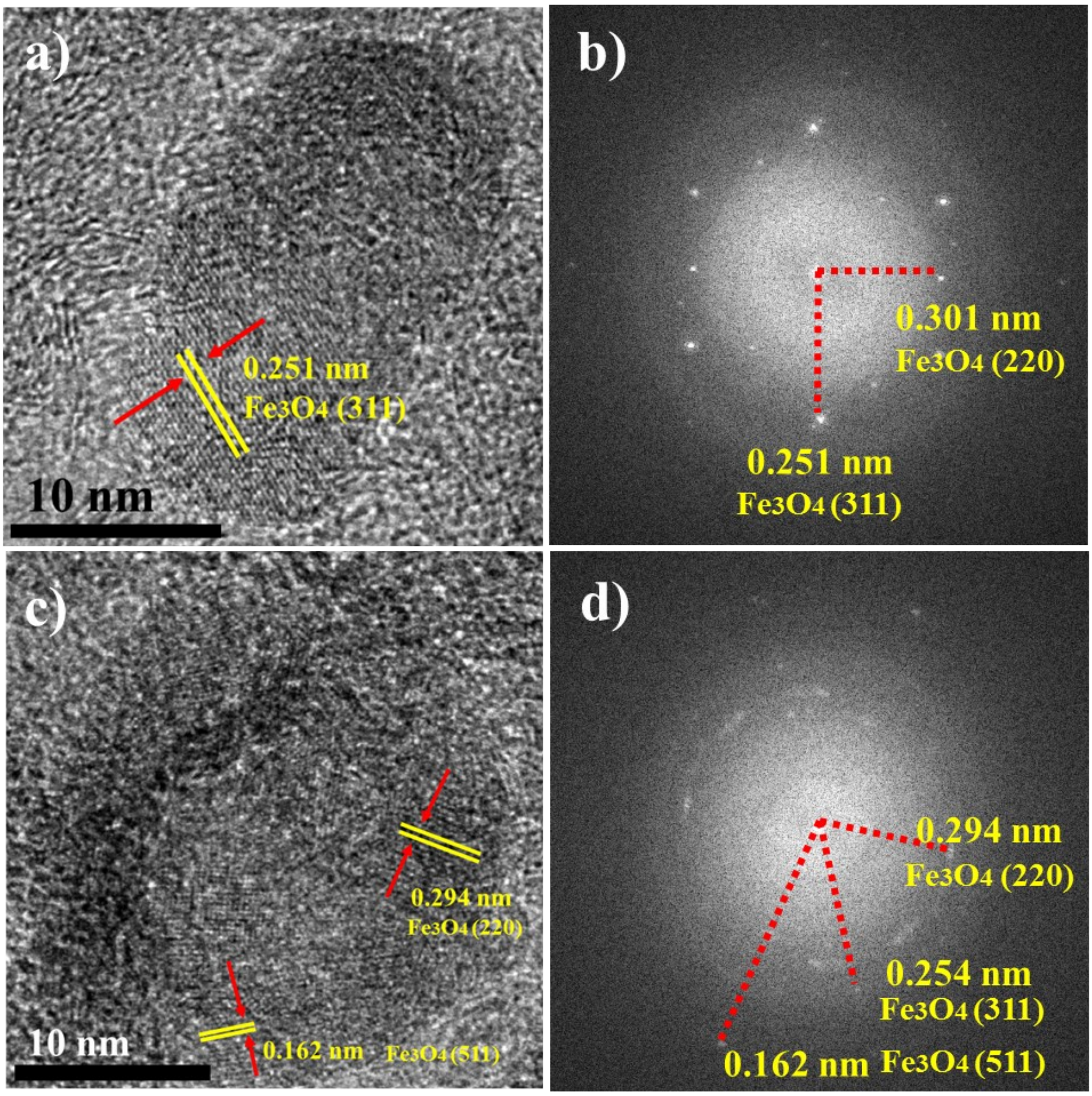

Figure. S7 HRTEM images and corresponding FTT images of (a-b) Fe_2O_3@NC-350 and (c-d) Fe_2O_3@NC-550.

Table S2 - Surface composition of the as-prepared catalysts.

Element	Fe_2O_3@NC-0	Fe_2O_3@NC-350	Fe_2O_3@NC-450	Fe_2O_3@NC-550	Fe_2O_3@NC-650
C 1s	80.9	83.6	86.1	87.5	81.6
N 1s	6.9	6.9	6.5	6.0	5.5
O 1s	10.5	8.2	6.3	5.4	11.9
Fe 2p	1.7	1.3	1.1	1.1	1.0

Table S3 - The ratio of different N species on the surfaces of different catalysts by XPS analysis.

Element	Fe_2O_3@NC-0	Fe_2O_3@NC-350	Fe_2O_3@NC-450	Fe_2O_3@NC-550	Fe_2O_3@NC-650
Pyridinic N	29.11	26.25	27.11	34.92	29.54
Pyrrolic N	20.86	19.98	18.20	16.01	17.46
Graphitic N	36.45	39.99	41.57	41.65	41.15
Oxidized N	13.58	13.78	13.12	7.42	11.85

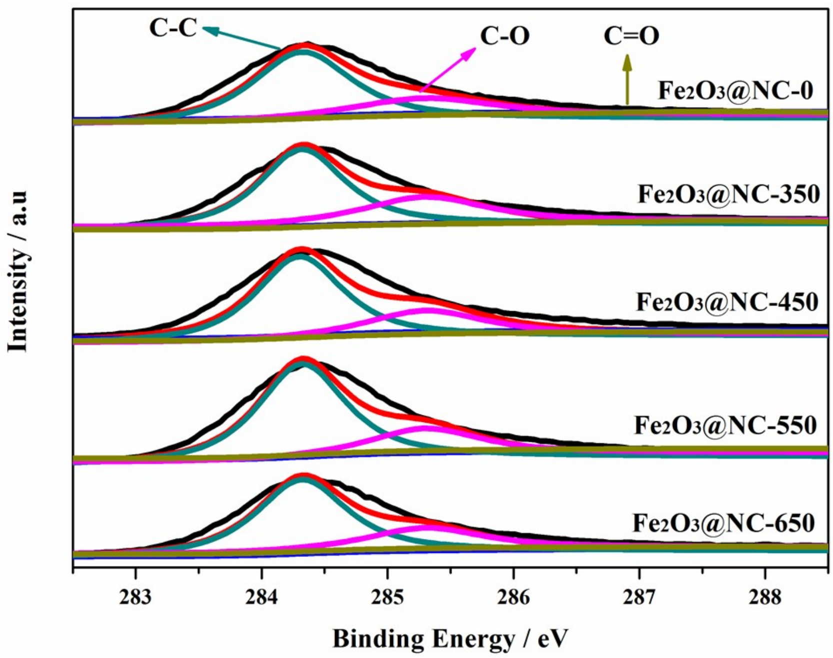

Figure. S8 C 1s XPS spectra of the as-prepared samples.

Table S4-ORR activities of the catalysts in this study.

Catalysts	CV peak (V. vs RHE)	E_{onset} (V. vs RHE)	$E_{1/2}$ (V. vs RHE)	J_L mA cm^{-2}
Fe_2O_3@NC-0	0.811	0.997	0.851	6.12
Fe_2O_3@NC-350	0.824	1.000	0.842	6.34

Fe_2O_3@NC-450	0.829	1.001	0.838	6.71
Fe_2O_3@NC-550	0.839	1.002	0.844	5.80
Fe_2O_3@NC-650	0.844	0.998	0.846	5.69
20 wt% Pt/C	0.826	0.994	0.828	5.19

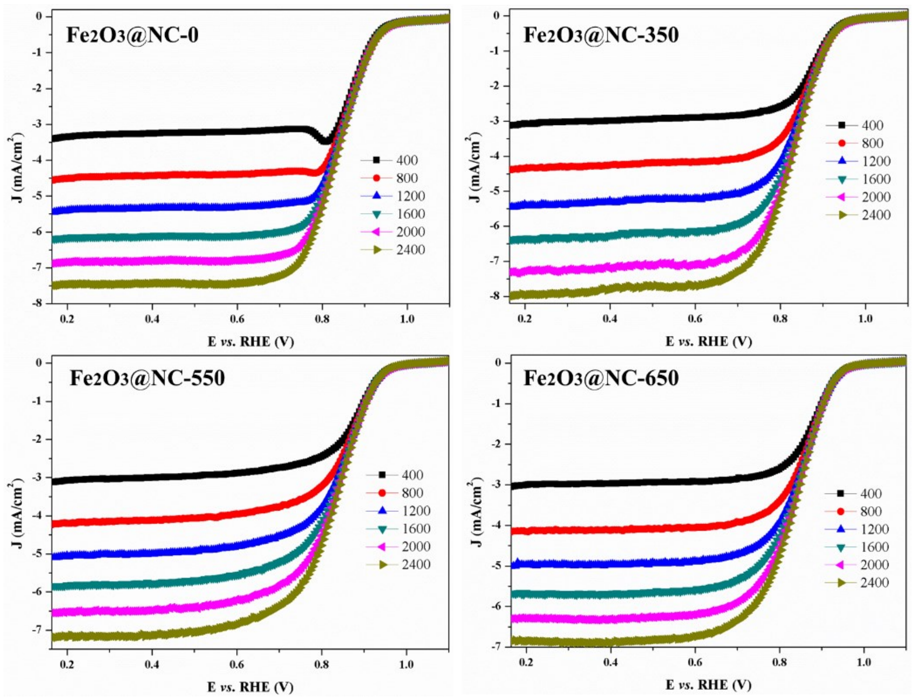

Figure. S9 Linear sweep voltammograms recorded in O_2-saturated 0.1 M KOH at a scan rate of 10 mV s^{-1}.

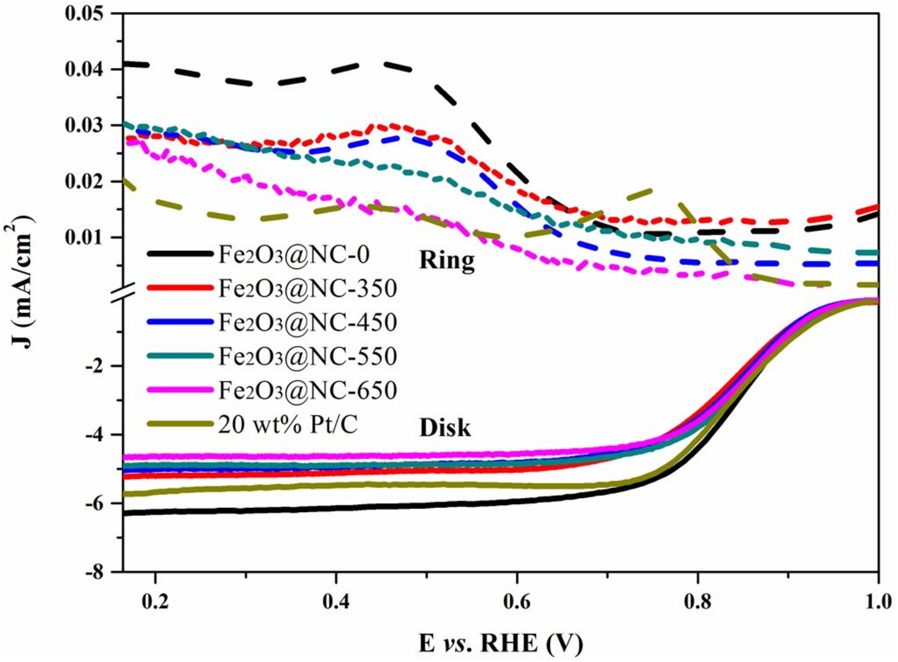

Figure. S10 RRED of ring and disk current.

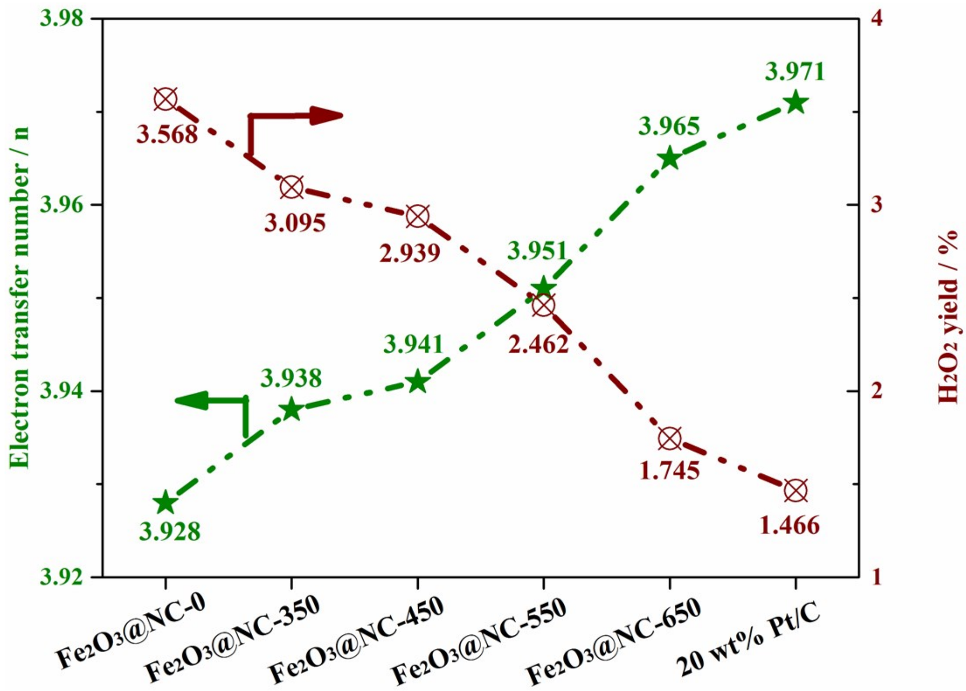

Figure. S11 Electron transfer number and H_2O_2 yield (0.45 V. RHE) on various catalysts.

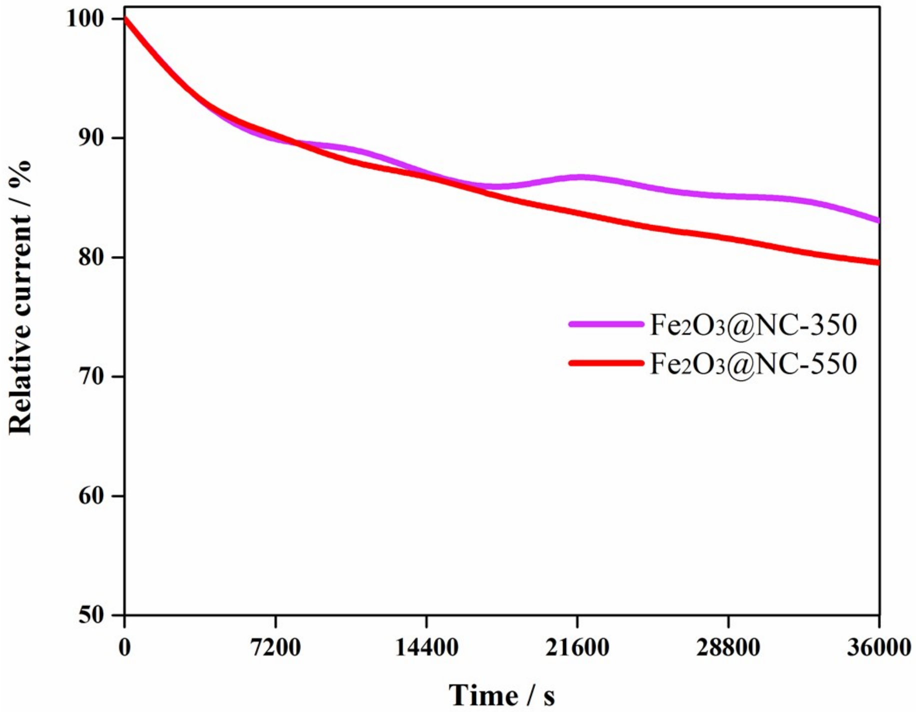

Figure. S12 Durability of Fe_2O_3@NC-350 and Fe_2O_3@NC-350 under O_2-saturated KOH solution (0.1 M).

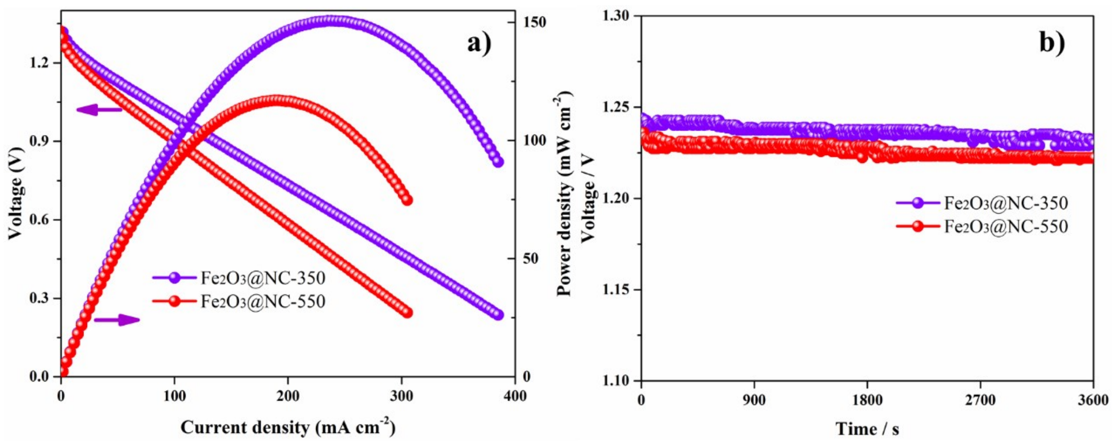

Figure. S13 (a) Polarization and power density curves of the zinc-air batteries using Fe_2O_3@NC-T (350 and 450) and 20 wt% Pt/C as the cathode catalyst. (b) Initial discharge for zinc-air test of Fe_2O_3@NC-T (350 and 450).

Table S5 - The peak power density and corresponding current density.

Catalysts	Peak power density (mW cm^{-2})	Current density (mA cm^{-2})
Fe_2O_3@NC-0	98.2	158.3
Fe_2O_3@NC-350	150.6	235.0
Fe_2O_3@NC-450	156.6	255.0
Fe_2O_3@NC-550	117.0	188.3
Fe_2O_3@NC-650	101.4	165.0
20 wt% Pt/C	68.0	98.5

Table S6 - Comparison of zinc-air performance between Fe_2O_3@NC-450 and those reported previously in other's works.

Catalysts	Loading (mg cm^{-2})	Power density (mW cm^{-2})	Relative to 20 wt% Pt/C	Refs.
Fe-N-CNBs-600	1.000	257	1.29	1
m-FeSNC	2.000	221	1.24	2
6%Fe-S-N CNN	1.000	132	1.81	3
CoFe/N-GTC	1.000	203	1.92	4
ZnCo@NC	1.200	152	1.47	5
Co/CoN_x/NC	-	96.6	0.99	6
Co/Co_3O_4/PGS	0.900	118.2	1.31	7
Co/Co-N-C	-	132	1.20	8
Co-SAs@NC	1.750	105.3	0.95	9
Fe@C_2N	1.000	123	1.06	10
Fe@FeNC	2.000	113	1.40	11
Fe/Fe_5C_2@NC	1.000	91	1.12	12
Fe/Fe_3C/NC	0.300	200	1.03	13
Fe/Fe_2O_3/FeNC	2.000	193	1.12	14
Fe_3O_4@NHCS-2	1.000	133	1.16	15

Fe_2O_3@NC-450	0.667	156.6	2.30	This work

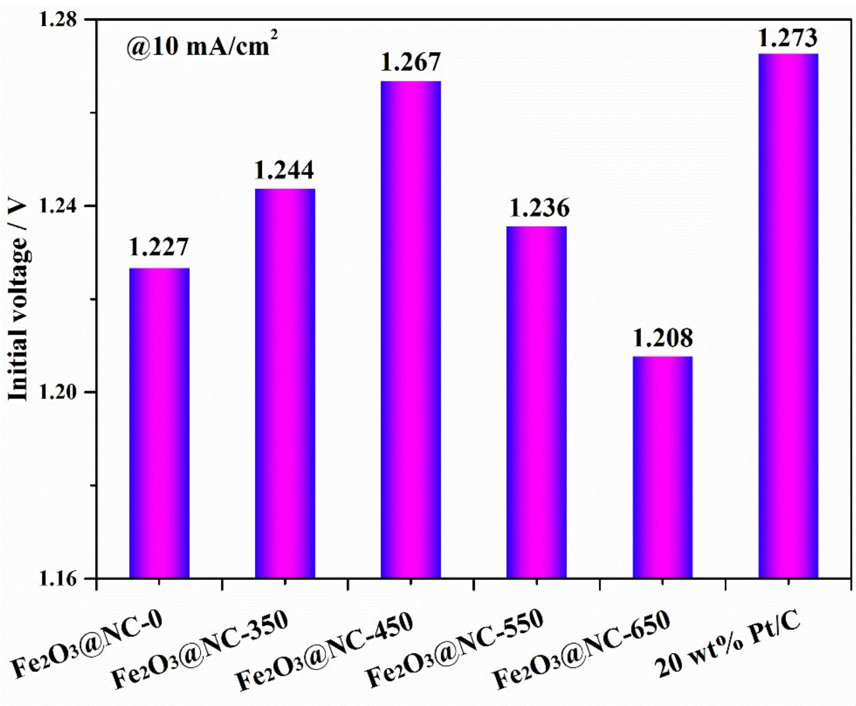

Figure. S14 Initial discharge for zinc-air test of Fe_2O_3@NC-T.

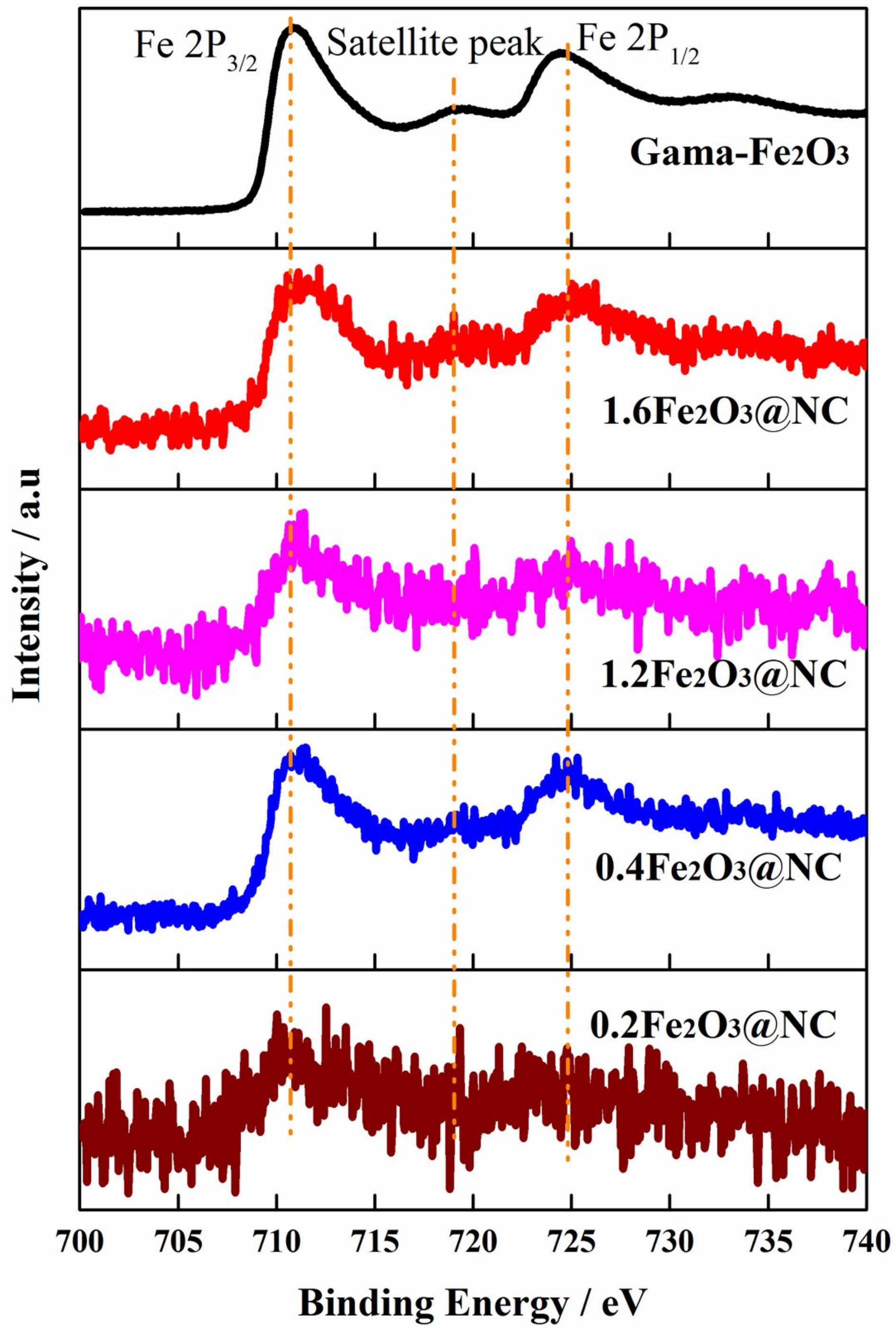

Figure. S15 XPS spectra of the Fe 2p core level region for the as-prepared catalysts.

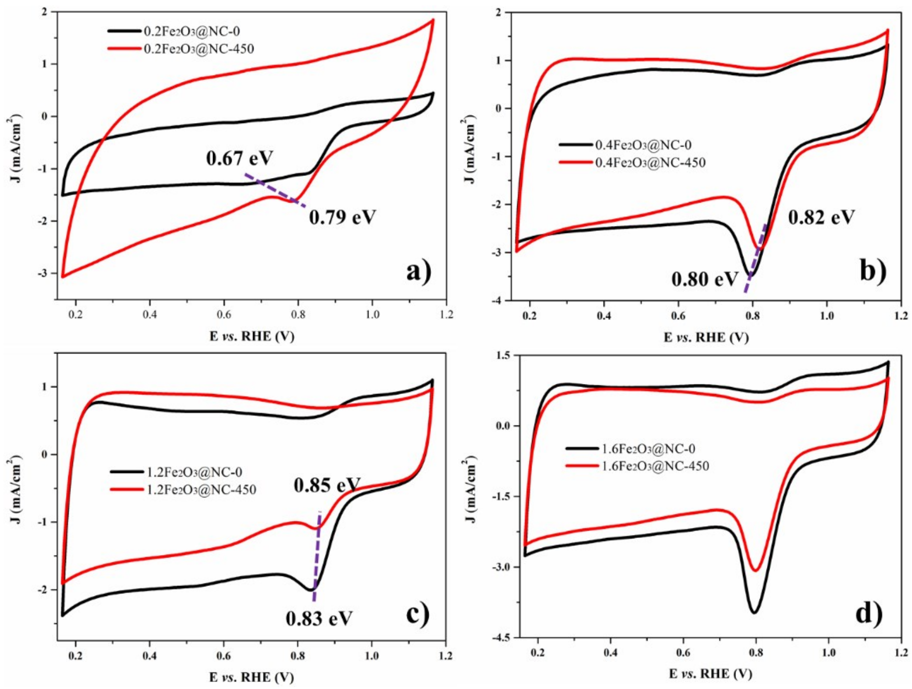

Figure. S16 Cyclic voltammograms of the catalysts prepared using different amounts of iron precursor and corresponding catalysts treated in H_2 atmosphere at 450 ^oC.

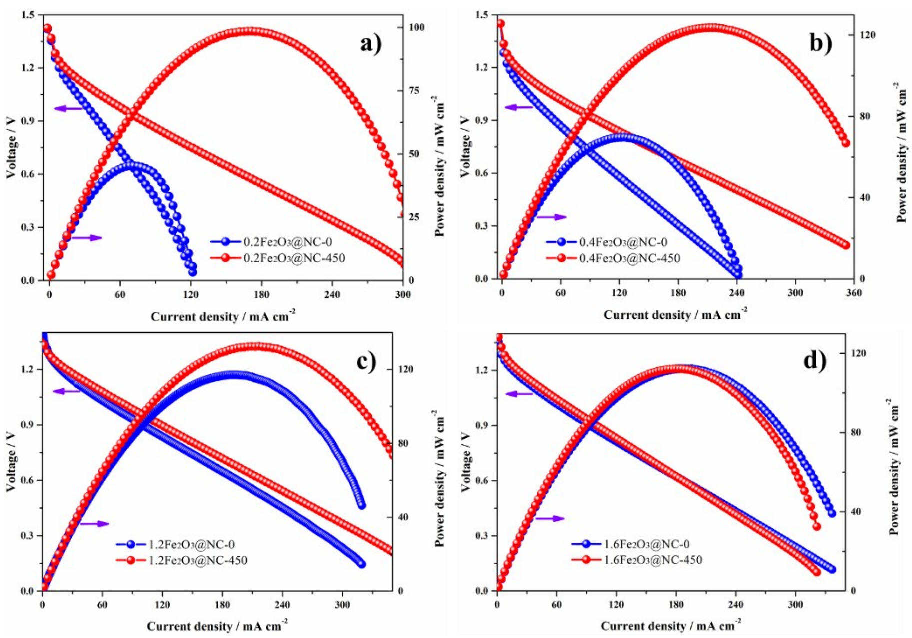

Figure. S17 Polarization and power density curves of the zinc-air batteries using the yFe_2O_3@NC-T catalysts and 20 wt% Pt/C as the cathode.

Table S7 - The peak power density and corresponding current density.

Catalysts	Peak power density ($mW\ cm^{-2}$)	Current density ($mA\ cm^{-2}$)
$0.2Fe_2O_3$@NC-0	45.3	71.7
$0.2Fe_2O_3$@NC-450	98.5	171.7
$0.4Fe_2O_3$@NC-0	69.6	125.0
$0.4Fe_2O_3$@NC-450	123.6	215.0
$1.2Fe_2O_3$@NC-0	117.1	191.9
$1.2Fe_2O_3$@NC-450	132.3	209.1
$1.6Fe_2O_3$@NC-0	112.3	186.2
$1.6Fe_2O_3$@NC-450	112.1	180.0

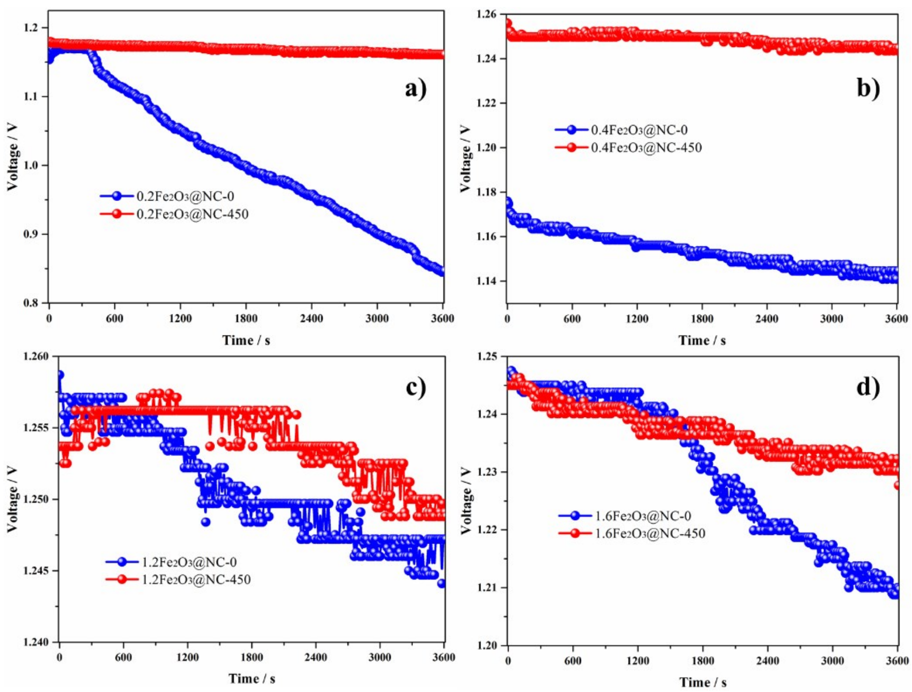

Figure. S18 The discharge curves of the zinc-air batteries using the yFe_2O_3@NC-T catalysts.

References

1. L. Cao, Z.-h. Li, Y. Gu, D.-h. Li, K.-m. Su, D.-j. Yang and B.-w. Cheng, *Journal of Materials Chemistry A*, 2017, **5**, 11340-11347.
2. Z. Guan, X. Zhang, W. Chen, J. Pei, D. Liu, Y. Xue, W. Zhu and Z. Zhuang, *Chemical communications*, 2018, **54**, 12073-12076.
3. H. Jin, H. Zhou, D. He, Z. Wang, Q. Wu, Q. Liang, S. Liu and S. Mu, *Applied Catalysis B: Environmental*, 2019, **250**, 143-149.
4. X. Liu, L. Wang, P. Yu, C. Tian, F. Sun, J. Ma, W. Li and H. Fu, *Angewandte Chemie*, 2018, **57**, 16166-16170.
5. B. Chen, X. He, F. Yin, H. Wang, D.-J. Liu, R. Shi, J. Chen and H. Yin, *Advanced Functional Materials*, 2017, **27**, 1700795.
6. C. Guan, A. Sumboja, W. Zang, Y. Qian, H. Zhang, X. Liu, Z. Liu, D. Zhao, S. J. Pennycook and J. Wang, *Energy Storage Materials*, 2019, **16**, 243-250.
7. Y. Jiang, Y.-P. Deng, J. Fu, D. U. Lee, R. Liang, Z. P. Cano, Y. Liu, Z. Bai, S. Hwang, L. Yang, D. Su, W. Chu and Z. Chen, *Advanced Energy Materials*, 2018, **8**, 1702900.
8. P. Yu, L. Wang, F. Sun, Y. Xie, X. Liu, J. Ma, X. Wang, C. Tian, J. Li and H. Fu, *Adv Mater*, 2019, **31**, e1901666.
9. X. Han, X. Ling, Y. Wang, T. Ma, C. Zhong, W. Hu and Y. Deng, *Angewandte Chemie*, 2019, **58**, 5359-5364.
10. F. L. Javeed Mahmood, Changmin Kim, Hyun-Jung Choi, Ohhun Gwon, and J.-M. S. Sun-Min Jung, Sung-June Cho, Young-Wan Ju, Hu Young Jeong, Guntae Ki, Jong-Beom Baek, *Nano Energy*, 2018, **44**, 304–310.
11. Z. Li, L. Wei, W.-J. Jiang, Z. Hu, H. Luo, W. Zhao, T. Xu, W. Wu, M. Wu and J.-S. Hu, *Applied Catalysis B: Environmental*, 2019, **251**, 240-246.
12. L. Song, T. Wang, L. Li, C. Wu and J. He, *Applied Catalysis B: Environmental*, 2019, **244**, 197-205.
13. G. S. P. Jang-Soo Lee, Sun Tai Kim, Meilin Liu,* and Jaephil Cho*, *Angew. Chem. Int. Ed.*, 2013, **52**, 1026-1030.
14. Y. Zang, H. Zhang, X. Zhang, R. Liu, S. Liu, G. Wang, Y. Zhang and H. Zhao, *Nano Research*, 2016, **9**, 2123-2137.
15. Y. Li, H. Huang, S. Chen, X. Yu, C. Wang and T. Ma, *Nano Research*, 2019, **12**, 2774-2780.